

RESEARCH

Open Access



# TNFRSF11B-modified umbilical cord mesenchymal stem cells as a novel strategy for bone-related diseases by suppressing osteoclast activity

Mina Ding<sup>1,2</sup>, Qian Ding<sup>2</sup>, Zhijie Liu<sup>2</sup>, Liang Wang<sup>2</sup>, Ke Pei<sup>2</sup>, Junyuan Hu<sup>2,3</sup>, Yan Liao<sup>2,3\*</sup> and Jian V. Zhang<sup>1,4,5\*</sup>

## Abstract

**Background and objective** Mesenchymal stem cells (MSCs), possessing multilineage potential, are capable of differentiating into osteoblasts and thus serve as suitable seed cells for bone regeneration. Tumor necrosis factor receptor superfamily member 11B (TNFRSF11B) gene encodes osteoprotegerin (OPG), which has a critical role in repressing osteoclast differentiation and has been reported to influence the adipogenic differentiation of bone marrow mesenchymal stem cells (BMMSCs). Nevertheless, the impact of TNFRSF11B on the osteogenic differentiation of umbilical cord mesenchymal stem cells (UCMSCs) remains unclear. This study aimed to investigate the role of TNFRSF11B in the osteogenesis of UCMSCs and bone remodeling.

**Methods** Differentially expressed genes (DEGs) were identified from the GEO database using R software. TNFRSF11B was transduced into UCMSCs by a lentiviral vector. Cell differentiation capacity was assessed by ALP staining, TRAP staining, and qRT-PCR assay. Proteomic analysis was performed to investigate the key proteins in TNFRSF11B-OE-UCMSCs that inhibit osteoclast differentiation.

**Results** We found that the TNFRSF11B gene was upregulated during osteogenic differentiation and downregulated during adipogenic differentiation of UCMSCs. UCMSCs overexpressing the TNFRSF11B gene were successfully generated via lentivirus transfection. However, neither the overexpression of TNFRSF11B nor treatment with exogenous OPG protein was sufficient to enhance the osteogenic potential of UCMSCs in vitro. Conditioned medium from TNFRSF11B-overexpressing UCMSCs significantly suppressed RANKL-induced osteoclast differentiation, while no significant effect was observed on osteoblast differentiation compared to the control group. Proteome analysis revealed that in the TNFRSF11B-OE-CM group, the expression of C1R, MDH1, and ACLY was significantly downregulated, while the expression of FETUB and METRNL was upregulated in the TNFRSF11B-OE-CM group, which was associated with the inhibition of osteoclast differentiation.

\*Correspondence:

Yan Liao

liaoyan@beike.cc

Jian V. Zhang

jian.zhang@siat.ac.cn

Full list of author information is available at the end of the article



© The Author(s) 2025. **Open Access** This article is licensed under a Creative Commons Attribution-NonCommercial-NoDerivatives 4.0 International License, which permits any non-commercial use, sharing, distribution and reproduction in any medium or format, as long as you give appropriate credit to the original author(s) and the source, provide a link to the Creative Commons licence, and indicate if you modified the licensed material. You do not have permission under this licence to share adapted material derived from this article or parts of it. The images or other third party material in this article are included in the article's Creative Commons licence, unless indicated otherwise in a credit line to the material. If material is not included in the article's Creative Commons licence and your intended use is not permitted by statutory regulation or exceeds the permitted use, you will need to obtain permission directly from the copyright holder. To view a copy of this licence, visit <http://creativecommons.org/licenses/by-nc-nd/4.0/>.

**Conclusion** This study demonstrates that although TNFRSF11B overexpression does not promote osteogenesis in UCMSCs, it may participate in regulating bone remodeling by inhibiting osteoclast differentiation.

**Keywords** Bone remodeling, TNFRSF11B, UCMSCs, Osteoclast differentiation

## Introduction

Mesenchymal stem cells (MSCs) possess pluripotency and have the capability to transform into various distinct cell lineages, encompassing osteoblasts, adipocytes, chondrocytes, myocytes, and even neurons, under suitable conditions [1, 2]. Accumulating evidence suggests that the pathways for osteogenic and adipogenic differentiation of MSCs are interconnected, with increased osteogenic differentiation corresponding to decreased adipogenic differentiation, and vice versa [3]. Impaired osteogenic differentiation of MSCs has been associated with bone disorders such as osteoporosis, which places a significant financial burden on patients and negatively affects their quality of life [4]. Therefore, maintaining a balance between the osteoblast and adipocyte differentiation of MSCs is crucial for supporting bone formation and overall skeletal health. A comprehensive understanding of the regulatory mechanisms governing this balance holds substantial medical significance for stem cell-based therapeutic strategies [5]. Additionally, bone remodeling is intricately regulated through the dynamic interplay between bone-forming osteoblasts and bone-resorbing osteoclasts [6]. Umbilical cord is normally discarded as medical waste. However, its derivatives, including umbilical cord mesenchymal stem cells (UCMSCs) and umbilical cord-derived Wharton's jelly, are frequently applied in regenerative medicine [7, 8]. Numerous studies have demonstrated that both UCMSCs and Wharton's jelly have significant potential in the treatment of bone-related diseases such as osteoporosis and osteoarthritis [9–12]. Yin Hu et al. have proposed that UCMSCs-derived extracellular vesicles contribute to bone metabolism by regulating the activities of both osteoclasts and osteoblasts [13][11]. Therefore, this study focused on UCMSCs and aims to identify proteins that enhance bone formation by directly promoting the differentiation of UCMSCs into osteoblasts or indirectly influencing bone remodeling, thereby providing potential therapeutic insights for bone-related diseases.

Osteoprotegerin (OPG), which is encoded by the tumor necrosis factor receptor superfamily member 11B (TNFRSF11B) gene, is predominantly synthesized and secreted by osteoblasts and osteocytes [14, 15] [13, 14]. The RANK/RANKL signaling system has been recognized as a key pathway in facilitating osteoclast formation and differentiation [16][15]. OPG competes with RANK for binding to RANKL, thereby suppressing osteoclast differentiation [13, 17] [16, 17]. The OPG/RANKL ratio is a critical determinant of bone mass and has been closely

linked to the development of osteoporosis [18]. Recent studies have revealed that OPG impedes the adipogenic differentiation of bone marrow mesenchymal stem cells (BMMSCs) [19]. Furthermore, TNFRSF11B-modified adipose-derived stem cells have been found to enhance bone formation in osteoporosis-induced rat models [20]. However, research has not yet investigated how the TNFRSF11B gene influences the osteogenic differentiation capacity of UCMSCs.

In the present study, TNFRSF11B expression was monitored throughout UCMSCs' transformation into both osteoblasts and adipocytes. Lentiviral transfection was employed to achieve TNFRSF11B overexpression. Upon verification that UCMSCs successfully overexpressed TNFRSF11B (TNFRSF11B-OE), the effects of TNFRSF11B overexpression and exogenous OPG protein on osteogenic differentiation of UCMSCs were assessed. Additionally, the impact of conditioned medium from TNFRSF11B-overexpressing cells (TNFRSF11B-OE-CM) and exogenous OPG protein on bone remodeling *in vitro* was investigated. Finally, proteomic analysis was performed to identify differentially expressed proteins (DEPs) between the TNFRSF11B-OE-CM and control-CM groups, aiming to elucidate the underlying mechanism by which TNFRSF11B-OE-CM inhibits osteoclast differentiation.

## Materials and methods

### Microarray analysis from the GEO database

To explore differentially expressed genes (DEGs) involved in MSC osteogenic and adipogenic differentiation, microarray data from the GEO database were analyzed using the GSE58919, GSE20045, GSE36923, and GSE37836 datasets procured (<https://www.ncbi.nlm.nih.gov/geo/>). RNA sequencing data from the database were utilized to identify DEGs before and after osteogenic and adipogenic induction. The Limma package in R language software was employed for subsequent analysis, with DEGs selected per the criteria of  $|\log_2 \text{fold change}| > 1$  and an adjusted  $P$ -value  $< 0.05$ .

### Cell culture

UCMSCs were obtained from Beike Biotechnology and maintained in MSC NutriStem<sup>®</sup> XF medium (Sartorius, Beit Haemek, Israel) supplemented with 1% human platelet lysate. Cells were incubated under controlled conditions (37 °C, 5% CO<sub>2</sub>), with medium replacement every 2–3 days. The expression of UCMSCs' surface markers was assessed via flow cytometry analysis. Positive

markers, including CD29, CD73, CD90, and CD117, were detected at levels exceeding 95%, whereas negative markers such as CD14, CD34, CD45, and CD117 were expressed at levels below 2%. All experiments were conducted using passage 8 cells. Ethical approval for this study was sanctioned by the Ethics Committee of Beike Biotechnology (No. BK-SL-20241018-01, Shenzhen, China).

#### MSCs differentiation assay

For UCMSCs differentiation experiments, 6-well plates were pre-coated with 1% gelatin and incubated at 37 °C for 30 min before cell seeding. To induce osteogenic differentiation, UCMSCs were seeded at a density of  $0.5 \times 10^5$  cells per well in 6-well plates. Cells were then incubated overnight at 37 °C in a humidified atmosphere with 5% CO<sub>2</sub>. The following day, cells were cultured in an osteogenic medium for 16 days. The differentiation medium was replaced every three days. The osteogenic medium was prepared using the MesenCult Osteogenic Differentiation Kit (Stem Cell Technologies). For lentivirus-transfected MSCs, the induction period was extended to 35 days to enhance osteogenic differentiation efficiency. For adipogenic differentiation, UCMSCs were seeded in 6-well plates at a density of  $0.5 \times 10^5$  cells per well and cultured with adipogenic differentiation medium the next day. The adipogenic medium was replaced every 3 days, and the culture was maintained at 37 °C for 25 days. The differentiation process was performed according to the protocol of the MesenCult Adipogenic Differentiation Kit. Following differentiation, the cells were utilized for subsequent experiments.

#### Alkaline phosphatase staining and Alizarin red staining

Following osteogenic differentiation, UCMSCs were subjected to staining using either the ALP or ARS staining kit (Beyotime, Shanghai, China). The experimental procedures were conducted as previously described [21]. Briefly, cells underwent washing with phosphate-buffered saline (PBS), underwent fixation using 4% paraformaldehyde for 30 min, and were subsequently washed three times with double-distilled H<sub>2</sub>O. Following this, BCIP/NBT solution or Alizarin Red S solution was introduced, and samples were maintained at ambient conditions for 30 min. Finally, cells underwent additional washing with double-distilled H<sub>2</sub>O and were examined under a microscope. The staining intensity of ALP or ARS was quantitatively assessed using ImageJ software.

#### Oil red O staining

The staining protocol followed the manufacturer's instructions for the Oil Red O staining kit (Beyotime, Shanghai, China). Following adipogenic differentiation, cells were processed as previously described. UCMSCs

were exposed to Oil Red O staining solution for 30 min. Finally, images were captured by an inverted fluorescence microscope.

#### Cell transfection

The lentiviral vectors pSLenti-EF1-EGFP-F2A-Puro-CMV-MCS-WPRE (control group) and pSLenti-EF1-EGFP-F2A-Puro-CMV-TNFRSF11B-WPRE (TNFRSF11B-OE group) were constructed, and the virus generation and viral titer assay were performed by Obio Technology (Shanghai, China). The viral titers of the control group and TNFRSF11B-OE group were  $4.01 \times 10^8$  TU/mL and  $2.60 \times 10^8$  TU/mL, respectively. UCMSCs were seeded into 6-well plates at a density of  $0.6 \times 10^5$  cells per well and incubated overnight at 37 °C. UCMSCs were then infected with lentivirus at an MOI of 30 and supplemented with polybrene-plus to enhance infection efficiency. After infection, cells were cultured in MSC medium containing 1 µg/ml puromycin for 2 days to select for puromycin-resistant cells. Fluorescent expression in the cells was detected using a fluorescence microscope. The gene and protein expression levels were examined via quantitative real-time polymerase chain reaction (qRT-PCR), Western blot, and enzyme-linked immunosorbent assay (ELISA) assays.

#### Western blot analysis

Cells underwent washing with cold PBS and were subjected to lysis using RIPA buffer (Beyotime, Shanghai, China) on ice conditions for 30 min, followed by a centrifugation step at  $12,000 \times g$  for 10 min at 4 °C. A bicinchoninic acid (BCA) protein assay kit (Beyotime, Shanghai, China) was employed to measure protein concentration. Equal quantities of protein samples underwent separation through 10% sodium dodecyl sulfate-polyacrylamide gel electrophoresis before transfer onto polyvinylidene fluoride membranes. The membranes were blocked using 5% skim milk and subsequently incubated with primary antibodies at 4 °C overnight. The study employed primary antibodies against OPG (1:1000, Abcam, ab183910) and β-actin (1:2000; Abclonal, Wuhan, China). After washing with phosphate-buffered saline with Tween, the membranes underwent incubation with an anti-rabbit or anti-mouse IgG secondary antibody (1:3000; Abclonal) for one hour at ambient conditions. Finally, the bands were detected using the BeyoECL Plus solution (Beyotime, Shanghai, China).

#### ELISA assay

The culture supernatant from UCMSCs in different experimental groups was collected. The concentration of OPG in the culture supernatant was quantified using an ELISA kit (Boster Biological Technology, Wuhan, China) per the supplier's protocol. Initially, the diluted sample

and protein standard were added to the ELISA plate for coating. Subsequently, a biotin-labeled antibody was introduced. The plate underwent triple rinsing with tris-buffered saline (TBS) before the avidin-peroxidase complex was applied. After five additional washes with TBS, the tetramethylbenzidine substrate solution was added to initiate color development, followed by incubation at 37 °C in the dark for 30 min. The process was halted by introducing a stop solution, and absorbance was measured at 450 nm. A serial dilution of the OPG protein standard was prepared, with concentration (pg/mL) plotted on the horizontal axis and optical density 450 nm values on the vertical axis. These parameters were utilized to generate the standard curve, which was subsequently employed to ascertain the OPG protein level in the test samples. Finally, the secretion levels of cellular OPG protein following lentiviral transfection were quantitatively assessed.

#### Osteoblast and osteoclast cell culture and treatment with UCMSCs-conditioned medium (UCMSCs-CM)

The transfected UCMSCs from both groups were cultured, and UCMSCs-CM was collected and prepared. Before storage or use, CM samples underwent filtration through a 0.2 µm membrane. FOB1.19 cells were maintained in modified D-modified Eagle's medium-F12 (DMEM-F12) comprising 10% fetal bovine serum (FBS) and 1% penicillin-streptomycin (P/S) in an incubator set at 34 °C with 5% CO<sub>2</sub>. Similarly, THP-1 cells were grown in RPMI 1640 medium comprising 10% FBS and 1% P/S. During differentiation, FOB1.19 or THP-1 cells

were exposed to either control-CM or TNFRSF11B-OE-CM derived from UCMSCs. For osteogenic induction, FOB1.19 cells underwent incubation in the osteogenic medium at 37 °C. For osteoclast induction, THP-1 cells received treatment with 100 ng/mL PMA over three days before being cultured in osteoclast differentiation medium supplemented with 100 ng/mL M-CSF and 100 ng/mL RANKL (PeproTech, New Jersey, United States). Finally, the influence of TNFRSF11B-OE-CM on osteoblast and osteoclast differentiation potential was assessed through subsequent experiments.

#### TRAP staining and TRAP activity assay

For the TRAP staining assay, cells were stained using a Tartrate-Resistant Acid Phosphatase (TRAP) Stain Kit (Solarbio, Cat. No. G1492, Beijing, China). The cells underwent fixation with a TRAP fixation solution, followed by two PBS washes. Subsequently, a TRAP staining solution was applied, followed by hematoxylin restaining and a 10-minute rinse with tap water. Finally, a microscopic examination was executed to obtain images, and TRAP-positive multinucleated cells were enumerated. To evaluate TRAP activity, specimens underwent lysis in RIPA buffer and centrifugation at 8000 g for 10 min at 4 °C. The measurement of TRAP activity utilized TRAP activity assay kits (Elabscience, Cat. No. E-BC-K871-M, Wuhan, China), with absorbance readings obtained at 405 nm via microplate reader. The TRAP activity measurements were standardized against the total protein content per sample.

#### RNA extraction and qRT-PCR

Total RNA was isolated utilizing TRIzol reagent (Invitrogen, CA, USA). The conversion of RNA to complementary DNA (cDNA) was executed employing the PrimeScript™ RT Reagent Kit (TaKaRa, Tokyo, Japan) with a gDNA Eraser present. The protocol for cDNA generation proceeded under these parameters: 42 °C for 2 min, 37 °C for 30 min, and 85 °C for 15 s. The mRNA levels were quantified using SYBR Green Real-time PCR Master Mix (TOYOBO, Osaka, Japan) on a LightCycler detection system. Normalization of mRNA levels was carried out using glyceraldehyde-3-phosphate dehydrogenase (GAPDH) as the reference gene, and relative gene expression was determined by the 2<sup>-ΔΔCT</sup> method. The primer sequences are depicted in Table 1.

#### LC-MS/MS analysis of proteomics

Proteomic analyses were conducted on the conditioned medium (CM) of control-UCMSCs and TNFRSF11B-OE-UCMSCs. The cells underwent cultivation in 175 cm<sup>2</sup> flasks over 48 h. The obtained growth medium underwent centrifugation at 12,000 g for 10 min at 4 °C to remove cell debris. All specimens were preserved at

**Table 1** Primers for RT-PCR in this study

Gene name	Forward (5' to 3')	Reverse (5' to 3')
RUNX2	CCAGTATGAGAGTAGGTGTCC	GGGTAAGACTGGTCATAG-GACC
ALP	GCTGTAAGGACATCGCCTACCA	CCTGGCTTCTCGT-CACTCTCA
Osteocalcin	CGCTACTGTATCAATGGCTGG	CTCCTGAAAGCCGATGTG-GTCA
BSP	GGCAGTAGTACTCATCCGAAG	GAAAGTGTGGTATTCT-CAGCCTC
TNFRSF11B	GGTCTCTGCTAACTCAGAAAGG	CAGCAAACCTGAAGAAT-GCCTCC
PPAR <sub>γ</sub>	GGGATCAGCTCCGTGGATCT	TGCACTTTGGTACTCTT-GAAGTT
FABP4	ACTGGGCCAGGAATTTGACG	CTCGTGAAGTGACGCCTT
CTSK	GAGGCTTCTCTGTGTCCATAC	TTACTGCGGAATGAGACAGGG
CTR	CCTGGAGACCTTCCAACAAGATG	CATTGGCGCTTACGGTG-GTTT
MMP9	GCCACTACTGTGCCTTTGAGTC	CCCTCAGAGAATCGC-CAGTACT
GAPDH	GTCTCTCTGACTTCAACAGCG	ACCACCTGTGTCTG-TAGCCAA

–80 °C to maintain integrity until subsequent examination. Further proteome assessment was executed by PTM Bio. A BCA kit was utilized to measure protein levels. Identical quantities of each protein specimen underwent digestion with 5 mM dithiothreitol for 30 min at 56 °C, followed by modification with 11 mM iodoacetamide for 15 min under dark conditions. The modified specimens were placed in ultrafiltration tubes for FASP digestion. Initially, specimens underwent three washing cycles with 8 M urea at 12,000 g at ambient temperature for 20 min, followed by three washes using 200 mM TEAB. Trypsin addition occurred at a trypsin-to-protein mass proportion of 1:50 for overnight processing. Peptide extraction was achieved through centrifugation at 12,000 g for 10 min at ambient temperature, with this step repeated twice. The final peptide mixture underwent desalting using a Strata X SPE column.

The DIA-NN search engine (v.1.8) was employed to examine the DIA data. Mass spectra analysis was performed by searching against the Homo\_sapiens\_9606\_SP\_20231220.fasta database (20,429 entries) with an incorporated reverse decoy database. Variance analysis was conducted based on intensity values to assess between-group differences, and proteins satisfying the criteria (fold change > 1.5,  $P < 0.05$ ) were identified as DEPs. Furthermore, to elucidate the characteristics of these DEPs, sub-cellular localization annotation, Gene Ontology (GO) enrichment analysis, and Kyoto

Encyclopedia of Genes and Genomes (KEGG) pathway enrichment analysis were performed. Functional terms with a fold enrichment > 1.5 and a  $p$ -value < 0.05 were considered statistically significant.

### Statistical analysis

All data are denoted as the mean ± standard deviation. The results were analyzed using GraphPad Prism 6.0 (GraphPad Software, Inc., USA). Statistical comparisons were conducted through a two-tailed Student's  $t$ -test. A  $p$ -value of < 0.05 was deemed statistically significant across all experiments.

## Results

### TNFRSF11B expression is increased during osteogenesis and decreased during adipogenesis of UCMSCs

To identify key regulatory genes associated with osteogenic and adipogenic differentiation of MSCs, an analysis of the GEO database was conducted. The results of heatmap analysis are presented in Fig. 1. The heatmap illustrates the top 100 DEGs in MSCs before and after osteogenic and adipogenic induction, respectively (Fig. 1A, B). Notably, TNFRSF11B exhibited high expression following osteogenic differentiation, whereas its expression was relatively low after adipogenic differentiation in the GEO database.

To examine TNFRSF11B gene expression during MSC differentiation, UCMSCs were cultured and subjected

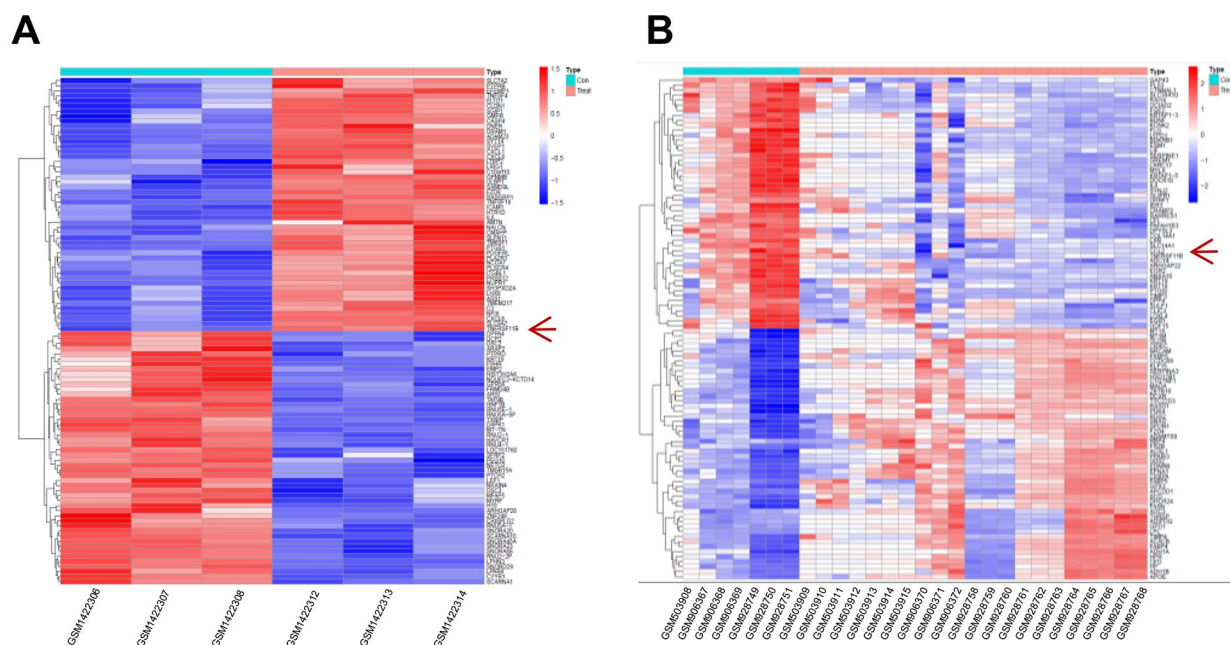


**Fig. 1** Identification of DEGs during adipogenesis and osteogenesis of MSCs in the GEO database. (A) Heatmap of DEGs between before and after MSC osteogenesis in GSE58919. (B) Heatmap of DEGs between before and after MSC adipogenesis in GSE20045, GSE36923, and GSE3783. Red arrows mark the TNFRSF11B gene

to osteogenic induction. ALP and ARS staining assays confirmed the activation of alkaline phosphatase and the formation of calcium nodules on the 16th day (Fig. 2A). qRT-PCR analysis revealed a significant upregulation of RUNX2, BSP, OCN, and TNFRSF11B gene expression on the 16th day (Fig. 2B). Additionally, the expression of TNFRSF11B following adipogenic differentiation of UCMSCs was assessed. Oil Red O staining demonstrated the presence of red lipid droplets on the 25th day after adipogenic induction (Fig. 2C). qRT-PCR results indicated a substantial increase in FABP4 and PPAR $\gamma$  gene expression, whereas TNFRSF11B expression was markedly reduced during adipogenic differentiation (Fig. 2D). These findings align with the previously observed

GEO database results, reinforcing the consistency of TNFRSF11B gene expression patterns.

#### TNFRSF11B does not affect the osteogenesis of UCMSCs and FOB1.19 cells

To confirm the role of TNFRSF11B in UCMSCs, TNFRSF11B-overexpressing UCMSCs were generated via lentiviral transfection. Fluorescence microscopy confirmed the presence of EGFP fluorescence expression in both groups of UCMSCs (Fig. 3A). qRT-PCR analysis revealed a significant upregulation of TNFRSF11B gene expression in UCMSCs compared to the control group, with OPG encoded by the TNFRSF11B gene (Fig. 3B). Western blot assay further demonstrated a substantial

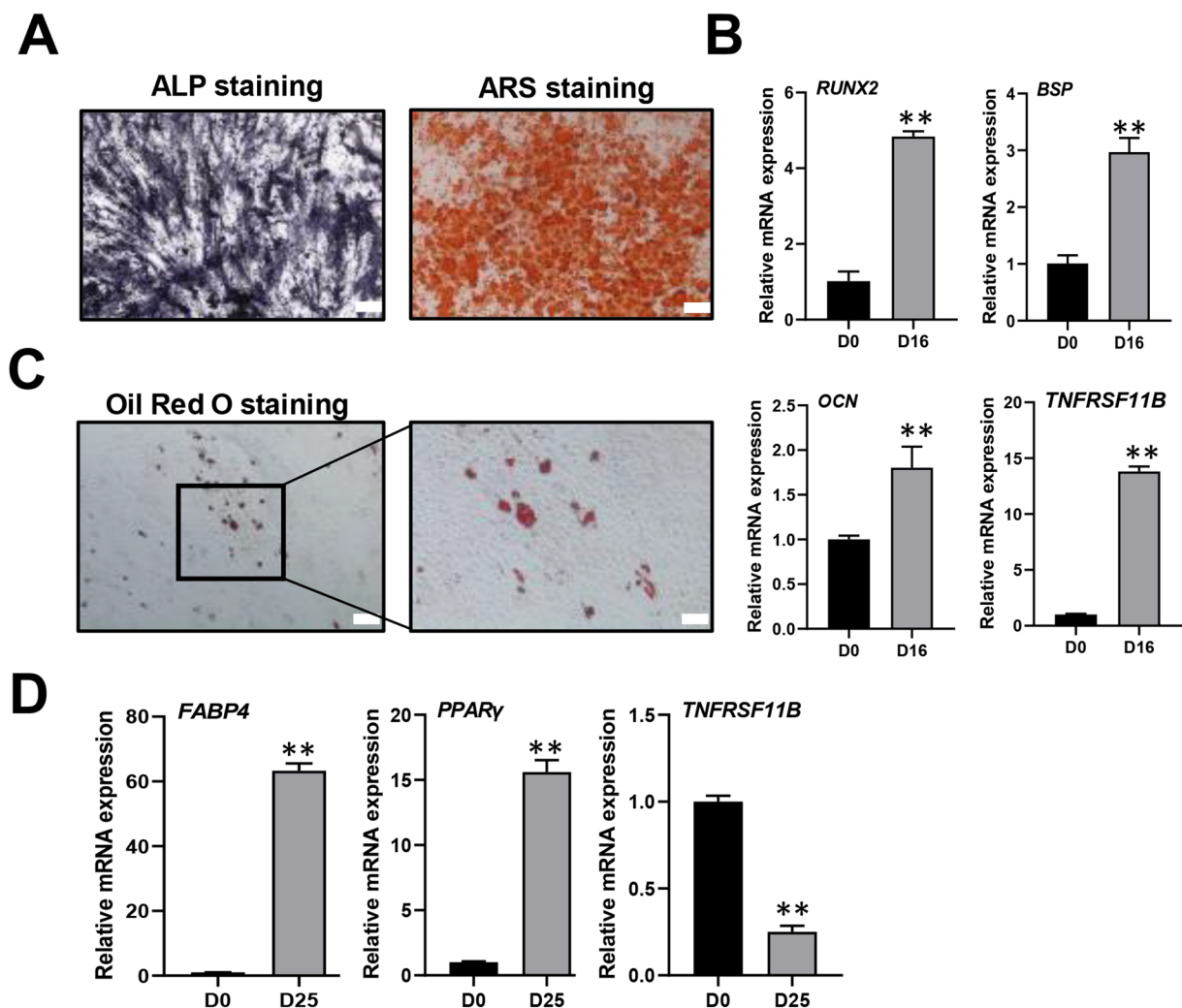


**Fig. 2** Expression of TNFRSF11B during adipogenesis and osteogenesis in UCMSCs. (A) Representative images of ALP and ARS staining in UCMSCs following osteogenic induction are shown (Scale bar: 200  $\mu$ m). (B) qRT-PCR analysis was conducted to assess the expression levels of RUNX2, BSP, OCN, and TNFRSF11B in UCMSCs cultured in osteogenic media for 16 days. (C) Representative images of Oil Red O staining in UCMSCs subjected to adipogenic induction for 25 days are displayed (Scale bar: left, 200  $\mu$ m; right, 100  $\mu$ m). (D) The mRNA expression levels of FABP4, PPAR $\gamma$ , and TNFRSF11B were quantified utilizing qRT-PCR. Expression levels were compared to day 0, \* $p < 0.05$ ; \*\* $p < 0.01$

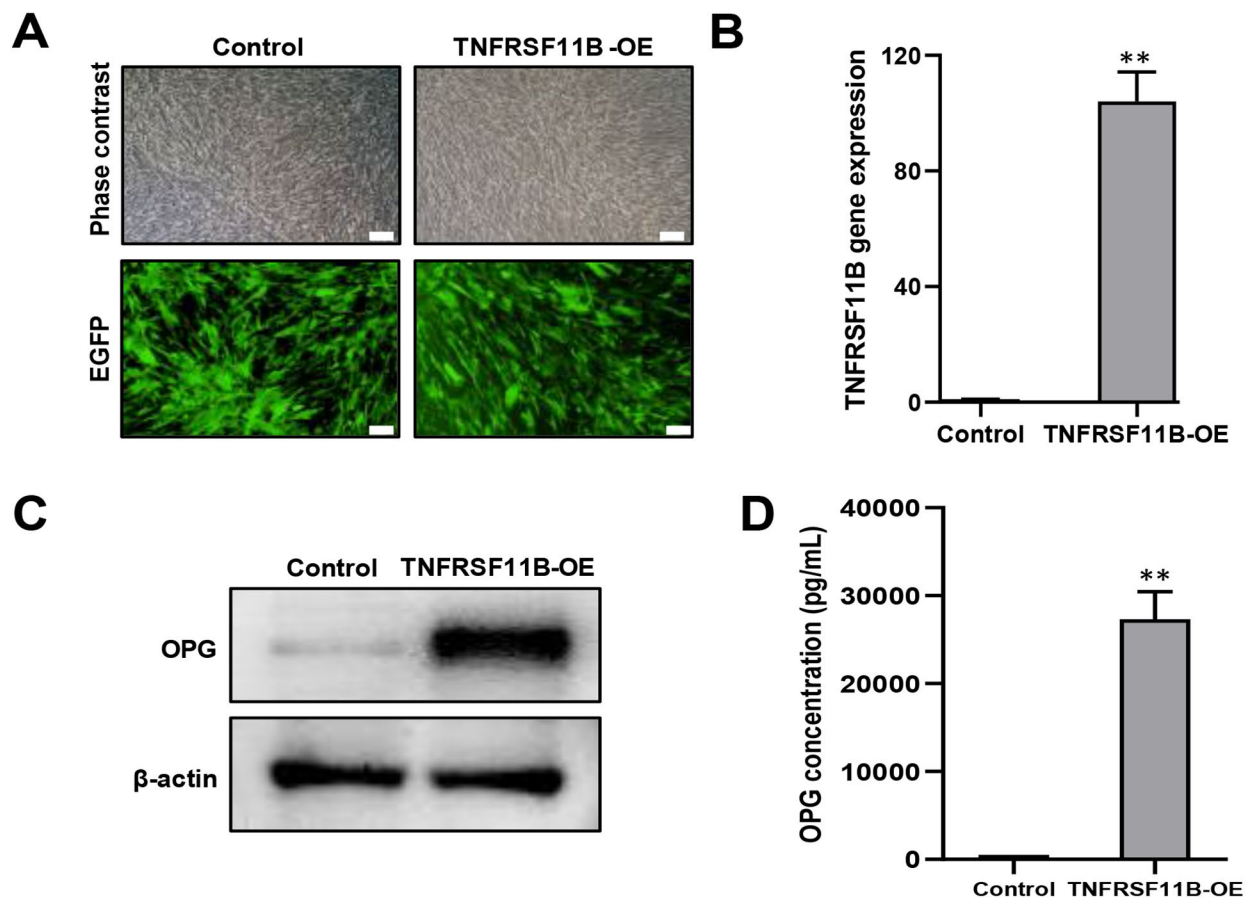


**Fig. 3** Lentivirus-mediated TNFRSF11B expression in UCMSCs. UCMSCs were transfected with TNFRSF11B overexpression (TNFRSF11B-OE) lentivirus or empty vector (control). (A) Representative images of phase contrast and immunofluorescence were taken with a microscope. (scale bar, 200  $\mu$ m) (B) TNFRSF11B mRNA levels in transfected UCMSCs were assessed by qRT-PCR analysis. (C) OPG protein expression in control or TNFRSF11B-OE UCMSCs was examined by Western blot assay. (D) The ELISA assay was performed to measure OPG levels in transfected UCMSCs. Compared with the control group, \* $p < 0.05$ ; \*\* $p < 0.01$

elevate in OPG expression relative to the control group (Fig. 3C). Additionally, ELISA results indicated that OPG protein levels in the supernatant of transfected UCMSCs were markedly elevated, reaching 27,300 pg/mL compared to the control (Fig. 3D). Collectively, these observations validate the successful construction of TNFRSF11B-overexpressing UCMSCs.

Subsequently, transfected UCMSCs were subjected to differentiation induction to examine the impact of TNFRSF11B overexpression on the osteogenic differentiation of UCMSCs. ALP staining results demonstrated that TNFRSF11B overexpression did not alter ALP activity (Fig. 4A, B). Furthermore, qRT-PCR analysis revealed that the mRNA expression levels of osteogenic differentiation-related markers, including RUNX2 and OCN, remained unchanged in response to TNFRSF11B overexpression, consistent with the ALP staining findings (Fig. 4C). In addition, the influence of human recombinant OPG protein on UCMSC osteogenesis was assessed.

ALP staining and qRT-PCR analysis indicated that exogenous OPG protein did not modulate the osteogenic differentiation of UCMSCs (Figure S1A-C). These findings confirm that neither TNFRSF11B overexpression nor exogenous OPG protein enhances the osteogenic differentiation of UCMSCs.

Bone remodeling is primarily governed by two key cell types: osteoblasts and osteoclasts [22]. To examine the impact of TNFRSF11B-overexpressing CM on osteoblasts, FOB1.19 cells were cultured and treated with CM derived from transfected UCMSCs (control-CM; TNFRSF11B-OE-CM). The findings revealed that ALP activity was increased in FOB1.19 cells in response to CM from transfected UCMSCs. Nevertheless, the control and TNFRSF11B-OE groups exhibited no substantial variations (Fig. 4D, E). Notably, qRT-PCR analysis suggested that osteogenesis-related gene levels (ALP, OCN) were downregulated in both conditions (Fig. 4F). Additionally, the osteogenic differentiation of FOB1.19 cells

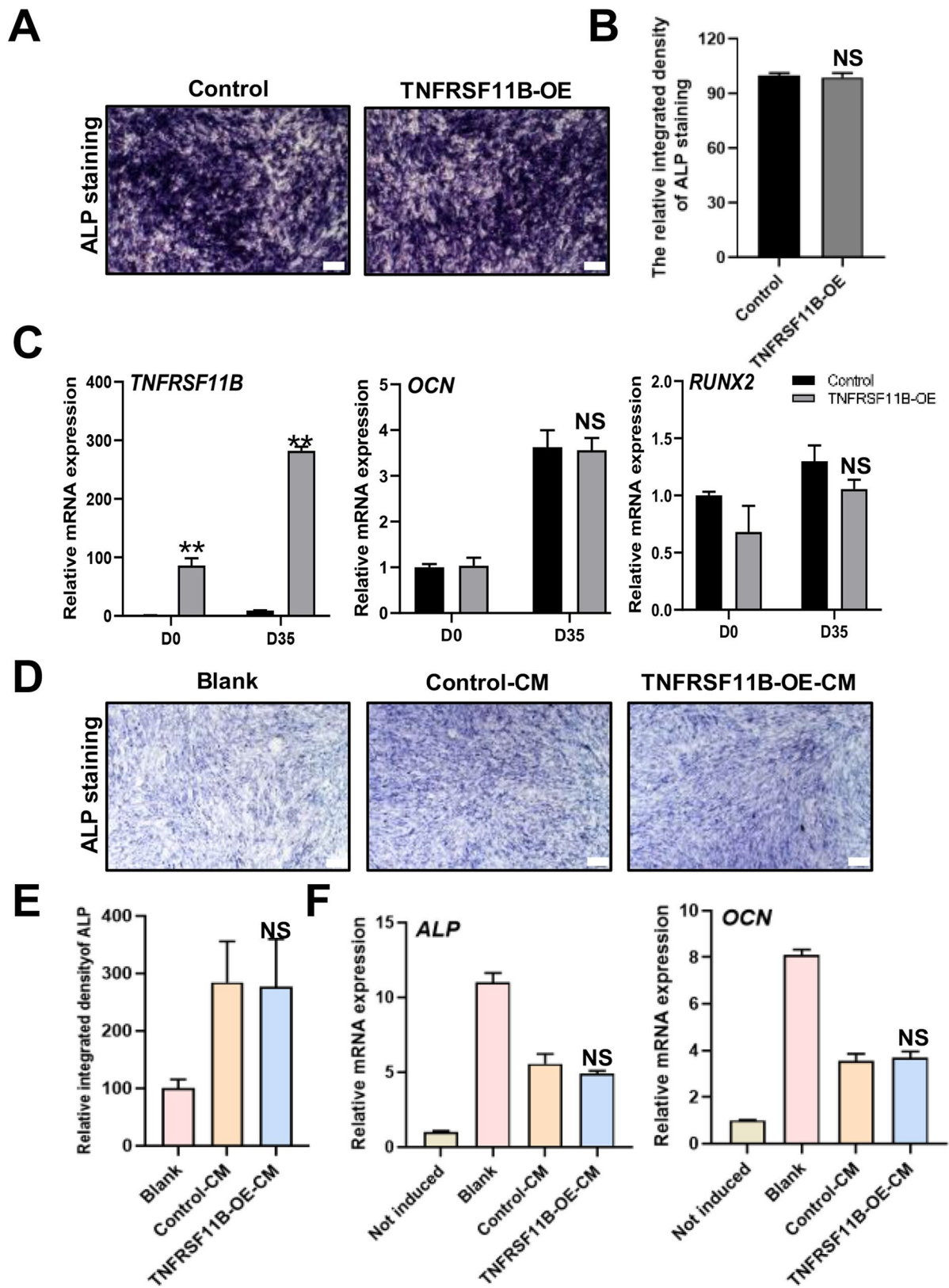


**Fig. 4** (See legend on next page.)

(See figure on previous page.)

**Fig. 4** The effect of TNFRSF11B overexpression on osteogenesis of UCMSCs and FOB1.19. (A) Representative images of ALP staining in control or TNFRSF11B-OE transfected UCMSCs following osteogenic induction (Scale bar: 200  $\mu$ m). (B) Quantification of ALP staining intensity was executed utilizing ImageJ software. (C) The expression levels of RUNX2, OCN, and TNFRSF11B in control and TNFRSF11B-OE UCMSCs were measured through qRT-PCR analysis. Comparisons were made to the control group. \* $p < 0.05$ ; \*\* $p < 0.01$ . (D) ALP staining of FOB1.19 cells treated with or without UCMSCs-CM (control-CM, TNFRSF11B-OE-CM) for 3 days (Scale bar: 200  $\mu$ m). (E) ALP staining intensity was quantified using ImageJ software. (F) The expression of osteogenesis-related genes in FOB1.19 cells, with or without control-CM and TNFRSF11B-OE-CM treatment, was examined by qRT-PCR. Blank represents the group without UCMSCs-CM treatment. Comparisons were made to the control group. NS: Not Significant

was assessed following treatment with 50 ng/mL recombinant OPG protein. The findings further confirmed that recombinant OPG protein did not enhance osteoblast differentiation (Figure S1D-F). These results suggest that the CM from TNFRSF11B-overexpressing UCMSCs is insufficient to promote osteoblast differentiation in FOB1.19 cells.

#### TNFRSF11B-modified UCMSCs suppress osteoclast differentiation through paracrine signaling

To further investigate whether TNFRSF11B overexpression in UCMSCs indirectly influences RANKL-induced osteoclast differentiation, THP-1 cells were treated with CM derived from transfected UCMSCs. Compared to cells treated with control-CM, TNFRSF11B-OE-CM reduced the formation rate of multinucleated osteoclasts (Fig. 5A, B). Additionally, a decrease in TRAP activity was observed in THP-1 cells treated with TNFRSF11B-OE-CM relative to those treated with control-CM (Fig. 5C). qRT-PCR analysis revealed that TNFRSF11B-OE-CM markedly downregulated the mRNA expression of osteoclast differentiation-related markers, including CTSK, MMP9, and CTR, compared to control-CM (Fig. 5D). Furthermore, a significant reduction in the expression levels of these genes was also detected in the recombinant OPG protein treatment group relative to the control group (Figure S2A-D). These findings indicate that both TNFRSF11B-OE-CM derived from UCMSCs and recombinant OPG protein exhibit comparable inhibitory effects on osteoclast differentiation.

#### Proteomics analyses of TNFRSF11B-OE-CM reveal DEGs mainly located in the extracellular region

To investigate the mechanism through which TNFRSF11B-OE-CM inhibits osteoclast differentiation, a label-free LC-MS/MS proteomic analysis was performed on the conditioned medium of transfected UCMSCs. A total of 820 proteins were identified, among which 810 were successfully quantified (Figure S3A). The majority of detected peptides ranged between 7 and 20 amino acids in length, aligning with established principles of trypsin hydrolysis and HCD fragmentation (Figure S3B). Pearson's correlation analysis and principal component analysis (PCA) revealed a strong and reproducible correlation between the protein content of the two groups (Figure S3C, D). Protein intensity distribution analysis across different samples indicated that protein quality

was consistently maintained across groups (Figure S3E). A heat map visualization depicts the DEPs in the TNFRSF11B-OE-CM group relative to the control-CM group (Fig. 6A). In total, 5 proteins were upregulated and 21 proteins were downregulated in the TNFRSF11B-OE-CM group compared to the control group (Fig. 6B). The relative expression levels of these DEPs are illustrated using a radar chart (Fig. 6C). Subcellular localization analysis revealed that DEPs were primarily distributed in the extracellular region, cytoplasm, plasma membrane, and nucleus, among other compartments (Fig. 6D). GO classification of DEPs indicated that they were predominantly involved in the regulation of biological processes (BP), extracellular region organization, and protein binding (Fig. 6E). These results indicated that the DEPs between the TNFRSF11B-OE-CM group and the control-CM group were mainly localized in the extracellular region.

#### GO and KEGG enrichment analysis of depts

To comprehensively assess the characteristics of DEPs, GO functional classification was conducted. The biological functions of DEPs were analyzed across three categories: BP, cellular component (CC), and molecular function (MF). Within the BP category, DEPs were predominantly associated with the oxaloacetate metabolic process, tricarboxylic acid metabolic process, and negative regulation of angiogenesis (Fig. 7A, B). In terms of CCs, DEPs were primarily localized in the extracellular region, extracellular matrix, intercellular bridge, and collagen trimer (Fig. 7C, D). Regarding MF, DEPs were mainly linked to peptidase activity, metalloendopeptidase activity, endopeptidase activity, and extracellular matrix structural constituents (Fig. 7E, F). Additionally, KEGG enrichment analysis of downregulated DEPs revealed their involvement in several intricate biological pathways, including the tricarboxylic acid cycle (TCA cycle), protein digestion and absorption, and systemic lupus erythematosus (Fig. 7G, H). Specifically, within the TCA cycle, MDH1 and ACLY were identified as the principal DEPs contributing to these pathways (Fig. 7I). These findings suggest that the effect of UCMSCs overexpressing TNFRSF11B on the osteoclast differentiation process may be closely associated with the extracellular matrix and TCA cycle. Furthermore, proteomic analysis demonstrated that overexpression of TNFRSF11B led to an increase in the expression intensity of OPG, Fetuin-B

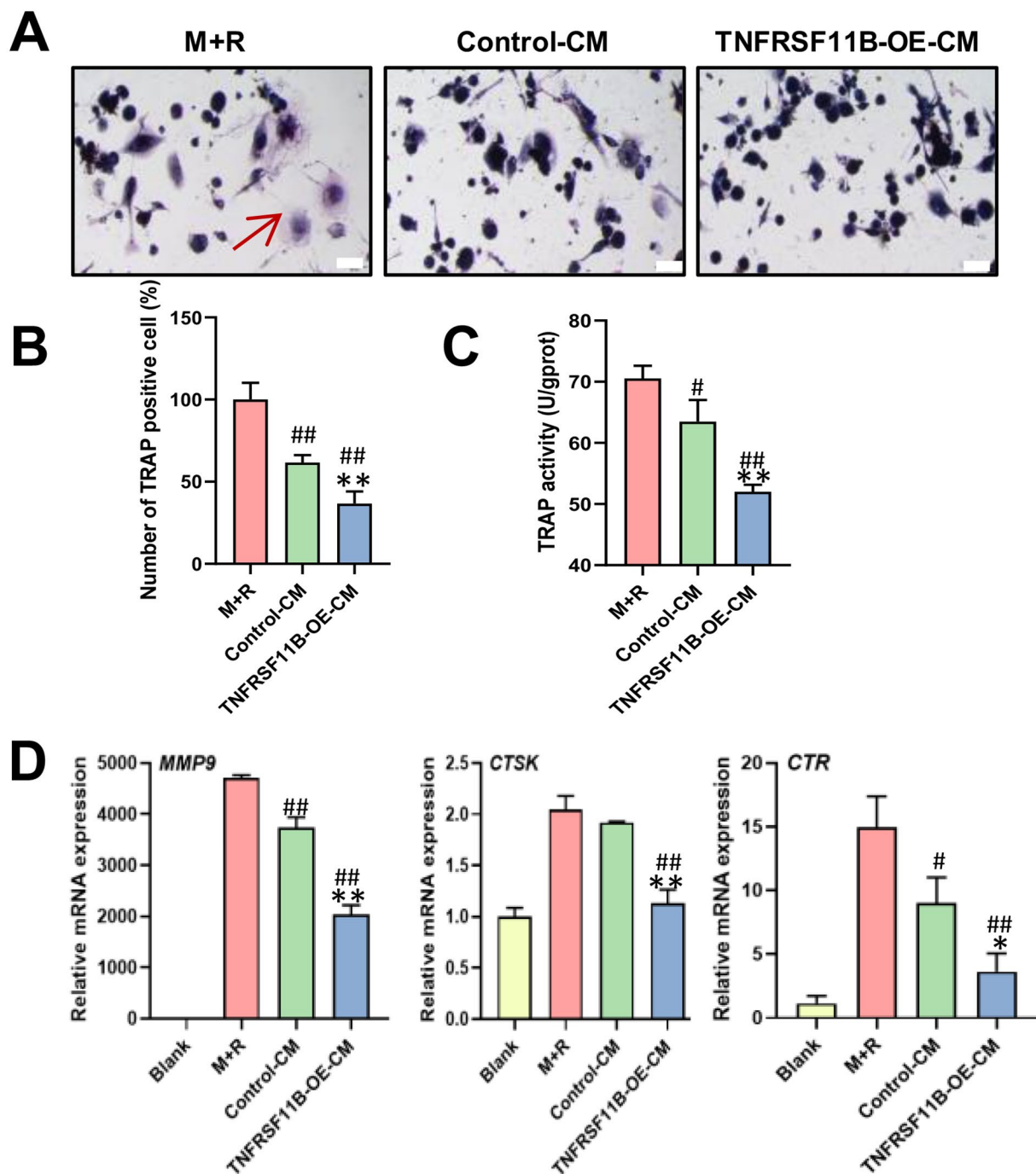


**Fig. 5** The effect of TNFRSF11B-OE-CM on the differentiation of osteoclasts. THP-1 cells were incubated with PMA for 3 days, followed by culture in the presence of M-CSF (100 ng/mL), RANKL (100 ng/mL), and either control-CM or TNFRSF11B-OE-CM for an additional 12 days. (A, B) Representative images of TRAP staining and corresponding statistical analysis illustrate the number of TRAP-positive multinucleated cells with differentiated osteoclasts marked by red arrows. (C) TRAP activity was quantified in THP-1 cells treated with control-CM or TNFRSF11B-OE-CM. (D) qRT-PCR analysis was conducted to assess the expression levels of osteoclast differentiation-related marker genes in each group. Blank represents the uninduced group. Comparisons were made relative to the M-CSF and RANKL (M+R) stimulation group, # $p < 0.05$ , ## $p < 0.01$ ; compared with the control-CM group, \* $p < 0.05$ ; \*\* $p < 0.01$

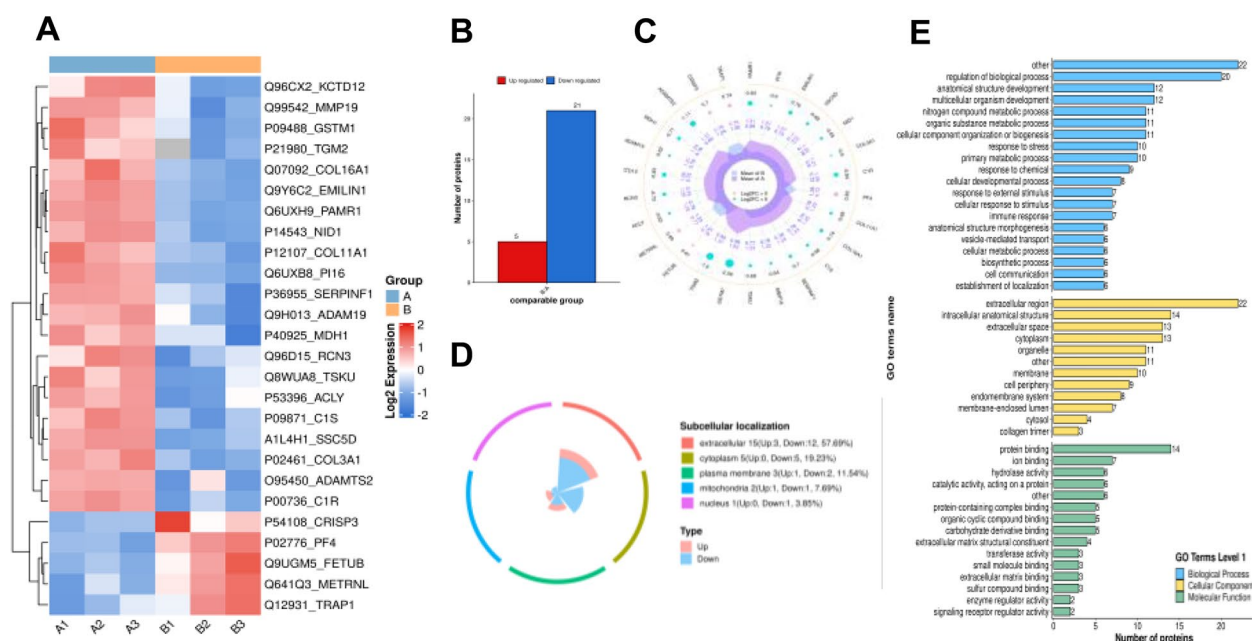


**Fig. 6** Proteomics analysis of the CM in control and TNFRSF11B-OE groups. (A, B) Differential protein expression between the two sample groups is depicted using a heat map and bar chart. In the heat map, blue represents downregulation, while red denotes upregulation. (C) The radar chart illustrates the relative expression levels of DEPs. The innermost circle ranks the differential proteins clockwise along the orange arrows based on p-values from smallest to largest. The second circle displays the Log<sub>2</sub>-transformed ratio, with pink indicating upregulation and light blue representing downregulation, while larger dots denote greater fold changes. The third circle indicates the average quantification level of the two groups, where spikes in the graph signify highly expressed differential proteins. (D) The figure presents the distribution of differential proteins across various subcellular structures, along with their proportional representation in each category. Pink indicates upregulated proteins, whereas blue represents downregulated proteins. (E) The GO secondary classification of DEPs. Capital letters "A" and "B" in (A–C) correspond to the control-CM and TNFRSF11B-OE-CM groups, respectively

(FETUB), and METRNL, while the expression levels of C1R, MDH1, and ACLY were reduced (Fig. 8). Notably, OPG expression was undetectable in the control group and, therefore, was not classified among the DEPs. These proteins have been previously implicated in the regulation of osteoclast differentiation. Collectively, these results suggest that TNFRSF11B-OE-CM may exert an inhibitory effect on osteoclast differentiation by modulating the expression of these key regulatory proteins.

## Discussion

The differentiation of MSCs into osteoblasts serves a fundamental function in bone formation and repair [23, 24]. Bone remodeling, a dynamic process essential for skeletal homeostasis, is regulated by the coordinated activities of osteoblasts and osteoclasts [25]. Dysregulation of bone remodeling homeostasis predisposes to skeletal pathologies such as osteoporosis and impaired fracture healing [4, 26]. Identifying key regulatory genes that promote MSC osteogenic differentiation or regulate bone remodeling processes is critical for advancing MSC-based therapeutic strategies against bone disorders [27]. Therefore, we genetically modified UCMSCs to investigate their regulatory roles in bone remodeling, thereby offering novel therapeutic possibilities for bone-related diseases.

In the present study, analysis of the GEO database revealed that TNFRSF11B exhibited upregulated expression during MSC osteogenic differentiation, while its expression was downregulated during MSC adipogenic differentiation. To validate these findings, the expression levels of TNFRSF11B during the osteogenic and adipogenic differentiation of UCMSCs were examined using qRT-PCR analysis. Consistent with the database findings, TNFRSF11B expression, aligned with osteogenesis-related genes (RUNX2, OCN, and BSP), was markedly upregulated in UCMSCs following osteogenic induction [28, 29]. Additionally, previous studies have identified FABP4 and PPAR $\gamma$  as key regulatory factors in MSC adipogenic differentiation [30, 31]. Unlike FABP4 and PPAR $\gamma$ , TNFRSF11B expression was significantly downregulated during UCMSCs adipogenic differentiation. These results demonstrated that TNFRSF11B expression was upregulated during the osteogenic differentiation and downregulated during adipogenic differentiation of UCMSCs, aligning with the data retrieved from the GEO database.

To investigate the impact of TNFRSF11B on the osteogenic differentiation of UCMSCs, we generated TNFRSF11B-overexpressing UCMSCs. Contrary to previous reports, overexpression of TNFRSF11B did



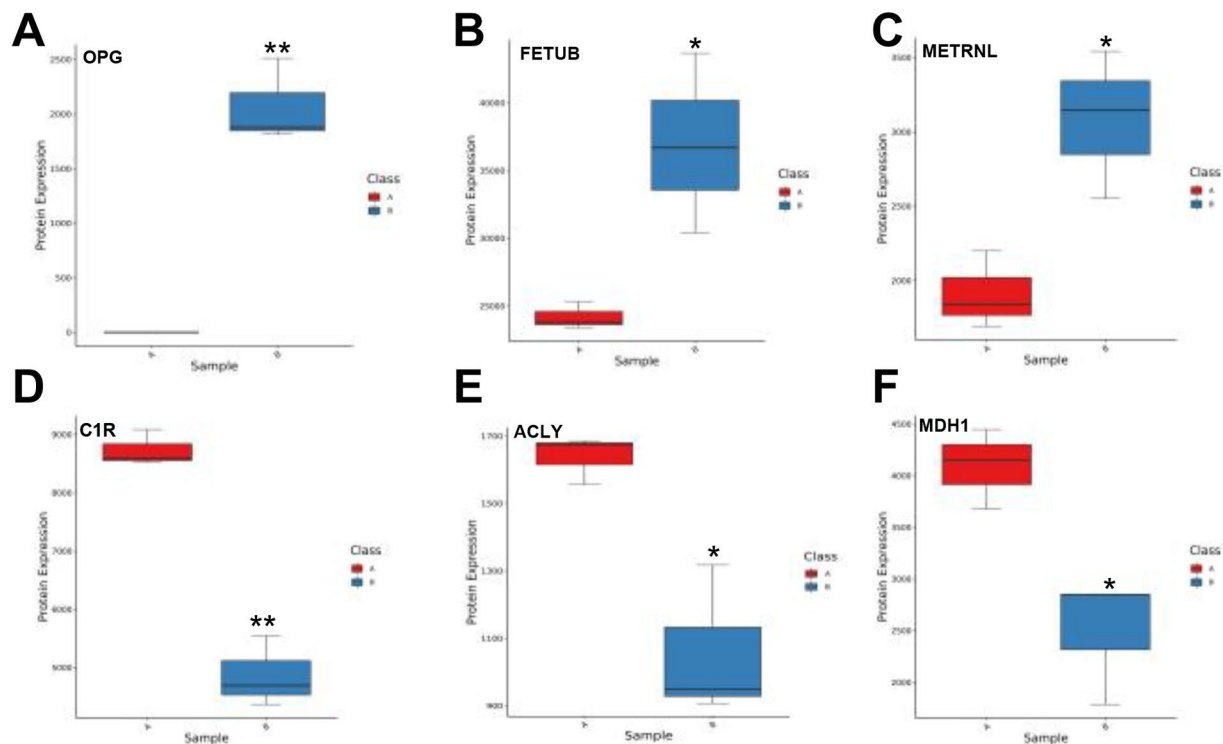


**Fig. 8** Intensity of DEPs in control-CM and TNFRSF11B-OE-CM groups. (A–F) Box plots illustrating the intensity variations of selected DEPs in the TNFRSF11B-OE-CM group relative to the control-CM group. \* $p$ -value < 0.05; \*\* $p$ -value < 0.01. Capital letters “A” and “B” in (A–F) correspond to the control-CM and TNFRSF11B-OE-CM groups, respectively

modulating osteoclast and osteoblast differentiation. In the present study, the TNFRSF11B-OE-CM group was markedly downregulated compared to the control-CM group, aligning with previous findings [36]. Recombinant OPG protein also suppressed osteoclast differentiation, though its inhibitory effect was less pronounced than that of TNFRSF11B-OE-CM. However, neither TNFRSF11B-OE-CM nor OPG protein promoted osteoblast differentiation, which is inconsistent with the findings of Kim J.H. et al. [37]. Notably, ALP and OCN gene expression was suppressed in control-CM and TNFRSF11B-OE-CM groups, though the underlying mechanism remains unclear. These unexpected results highlight certain limitations that require further investigation. These results demonstrated that while TNFRSF11B overexpression does not enhance the osteogenic differentiation of UCMSCs, it serves a regulatory function in bone remodeling by inhibiting osteoclast differentiation.

To elucidate the mechanism through which TNFRSF11B-OE-CM inhibits RANKL-induced osteoclast differentiation, a proteomics analysis was performed to identify DEPs in TNFRSF11B-OE-CM. The findings revealed that these proteins were predominantly localized to the extracellular matrix and enriched in pathways such as the TCA cycle and protein digestion/absorption.

Key downregulated proteins included C1R, MDH1, and ACLY, which are crucial regulators of osteoclast differentiation [38–40]. Furthermore, upregulated proteins such as FETUB and METRNL were associated with osteoclast signaling pathways, including the PI3K/AKT, AMPK, and NF- $\kappa$ B pathways [41–45]. These findings suggest that TNFRSF11B-OE-CM might suppress osteoclast differentiation by modulating extracellular matrix components and associated signaling pathways. However, the molecular mechanisms underlying TNFRSF11B-mediated regulation of these proteins in UCMSCs require further investigation. Additionally, the absence of *in vivo* functional validation is a limitation in this study. Future studies should further investigate the potential therapeutic effects of TNFRSF11B-modified UCMSCs for treating bone-related diseases.

In conclusion, this study demonstrated that TNFRSF11B expression was upregulated in osteogenic while downregulated in adipogenic UCMSCs. However, the overexpression of TNFRSF11B in UCMSCs did not enhance their osteogenesis differentiation potential. TNFRSF11B-OE-CM was indicated to inhibit osteoclast differentiation rather than promote bone formation. These findings provide valuable evidence for the TNFRSF11B-modified UCMSCs to participate in the

regulation of bone remodeling by inhibiting osteoclast differentiation.

### Supplementary Information

The online version contains supplementary material available at <https://doi.org/10.1186/s13018-025-05850-9>.

Supplementary Material 1

### Acknowledgements

We thank PTM Biolab (Hangzhou, China) for their technical support in proteomics analysis and Bullet Edits Limited for the linguistic editing and proofreading of the manuscript.

### Author contributions

Conceptualization, K.P., and M.D.; methodology, M.D.; software, Q.D.; validation, M.D., Z.L., and L.W.; formal analysis, M.D.; investigation, M.D.; resources, J.H.; data curation, M.D.; writing—original draft preparation, M.D.; writing—review and editing, Y.L. and J.Z.; visualization, M.D.; supervision, Y.L., and J.Z.; project administration, Y.L. and J.Z.; funding acquisition, J.H. All authors have read and agreed to the published version of the manuscript.

### Funding

This work was supported by the Guangdong Basic and Applied Basic Research Foundation (Grant no. 2024A1515030277), Beike Biotechnology Co., Ltd (Grant no. YF-016), Shenzhen Medical Research Fund (Grant no. B2404004), Shenzhen Key Laboratory of Metabolic Health (Grant No. ZDSYS20210427152400001), and Sino-European Center of Biomedicine and Health. The funding body played no role in the design of the study; the collection, analysis, or interpretation of the data; or the writing of the manuscript.

### Data availability

Sequence data that support the findings of this study have been deposited in the Proteomics Identification Database (PRIDE) with the primary accession code PXD062832.

### Declarations

#### Competing interests

The authors declare no competing interests.

#### Author details

<sup>1</sup>Shenzhen Key Laboratory of Metabolic Health, Center for Energy Metabolism and Reproduction, Shenzhen Institutes of Advanced Technology, Chinese Academy of Sciences, Shenzhen 518055, China

<sup>2</sup>Shenzhen Beike Biotechnology Co., Ltd, Shenzhen 518054, China

<sup>3</sup>Shenzhen Beike Biotechnology Research Institute, Shenzhen 518054, China

<sup>4</sup>Faculty of Pharmaceutical Sciences, Shenzhen University of Advanced Technology, Shenzhen 518055, China

<sup>5</sup>Sino-European Center of Biomedicine and Health, Shenzhen 518055, China

Received: 26 March 2025 / Accepted: 23 April 2025

Published online: 17 May 2025

### References

- Hoang DM, Pham PT, Bach TQ, Ngo ATL, Nguyen QT, Phan TTK, Nguyen GH, Le PTT, Hoang VT, Forsyth NR, et al. Stem Cell-Based therapy for human diseases. *Signal Transduct Target Ther*. 2022;7. <https://doi.org/10.1038/s41392-022-01134-4>.
- Robert AW, Marcon BH, Dallagiovanna B, Shigunov P. Adipogenesis, osteogenesis, and chondrogenesis of human mesenchymal stem/stromal cells: A comparative transcriptome approach. *Front Cell Dev Biol*. 2020;8:561. <https://doi.org/10.3389/fcell.2020.00561>.
- Chen Q, Shou P, Zheng C, Jiang M, Cao G, Yang Q, Cao J, Xie N, Velletri T, Zhang X, et al. Fate decision of mesenchymal stem cells: adipocytes or osteoblasts? *Cell Death Differ*. 2016;23:1128–39. <https://doi.org/10.1038/cdd.2015.168>
- Liang B, Burley G, Lin S, Shi Y-C. Osteoporosis pathogenesis and treatment: existing and emerging avenues. *Cell Mol Biol Lett*. 2022;27:72. <https://doi.org/10.1186/s11658-022-00371-3>.
- Hu L, Yin C, Zhao F, Ali A, Ma J, Qian A. Mesenchymal stem cells: cell fate decision to osteoblast or adipocyte and application in osteoporosis treatment. *Int J Mol Sci*. 2018;19:360. <https://doi.org/10.3390/ijms19020360>.
- Kim J-M, Lin C, Stavre Z, Greenblatt MB, Shim J-H. Osteoblast-Osteoclast communication and bone homeostasis. *Cells*. 2020;9:2073. <https://doi.org/10.3390/cells9092073>.
- Gupta A, El-Amin SF, Levy HJ, Sze-Tu R, Ibim SE, Maffulli N. Umbilical Cord-Derived Wharton's jelly for regenerative medicine applications. *J Orthop Surg Res*. 2020;15:49. <https://doi.org/10.1186/s13018-020-1553-7>.
- Rajput SN, Naeem BK, Ali A, Salim A, Khan I. Expansion of human umbilical cord derived mesenchymal stem cells in regenerative medicine. *World J Stem Cells*. 2024;16:410–33. <https://doi.org/10.4252/wjsc.v16.i4.410>.
- Gupta A, Maffulli N, Rodriguez HC, Lee CE, Levy HJ, El-Amin SF. Umbilical Cord-Derived Wharton's jelly for treatment of knee osteoarthritis: study protocol for a Non-Randomized, Open-Label, Multi-Center trial. *J Orthop Surg Res*. 2021;16:143. <https://doi.org/10.1186/s13018-021-02300-0>.
- Gupta A, Maffulli N. Allogenic umbilical cord tissue for treatment of knee osteoarthritis. *Sports Med Arthrosc Rev*. 2022;30:162–5. <https://doi.org/10.1097/JSA.0000000000000350>.
- Hu Y, Zhang Y, Ni C-Y, Chen C-Y, Rao S-S, Yin H, Huang J, Tan Y-J, Wang Z-X, Cao J, et al. Human umbilical cord mesenchymal stromal Cells-Derived extracellular vesicles exert potent bone protective effects by CLEC11A-Mediated regulation of bone metabolism. *Theranostics*. 2020;10:2293–308. <https://doi.org/10.7150/thno.39238>
- Gupta A, Maffulli N, Rodriguez HC, Carson EW, Bascharon RA, Delfino K, Levy HJ, El-Amin SF. Safety and efficacy of umbilical Cord-Derived Wharton's jelly compared to hyaluronic acid and saline for knee osteoarthritis: study protocol for a randomized, controlled, Single-Blind, Multi-Center trial. *J Orthop Surg Res*. 2021;16:352. <https://doi.org/10.1186/s13018-021-02475-6>.
- Udagawa N, Koide M, Nakamura M, Nakamichi Y, Yamashita T, Uehara S, Kobayashi Y, Furuya Y, Yasuda H, Fukuda C, et al. Osteoclast differentiation by RANKL and OPG signaling pathways. *J Bone Min Metab*. 2021;39:19–26. <https://doi.org/10.1007/s00774-020-01162-6>.
- Cawley KM, Bustamante-Gomez NC, Guha AG, MacLeod RS, Xiong J, Gubrij I, Liu Y, Mulkey R, Palmieri M, Thostenson JD, et al. Local production of osteoprotegerin by osteoblasts suppresses bone resorption. *Cell Rep*. 2020;32:108052. <https://doi.org/10.1016/j.celrep.2020.108052>.
- Fu Q, Bustamante-Gomez NC, Reyes-Pardo H, Gubrij I, Escalona-Vargas D, Thostenson JD, Palmieri M, Goellner JJ, Nookaew I, Barnes CL, et al. Reduced osteoprotegerin expression by osteocytes May contribute to rebound resorption after denosumab discontinuation. *JCI Insight*. 2023;8:e167790. <https://doi.org/10.1172/jci.insight.167790>.
- Takayanagi H. RANKL as the master regulator of osteoclast differentiation. *J Bone Min Metab*. 2021;39:13–8. <https://doi.org/10.1007/s00774-020-01191-1>.
- Tobeiha M, Moghadasian MH, Amin N, Jafarnejad S, RANKL/RANK/OPG. Pathway: A Mechanism Involved in Exercise-Induced Bone Remodeling. *Biomed Res Int* 2020, 2020, 6910312. <https://doi.org/10.1155/2020/6910312>
- Chi G, Qiu L, Ma J, Wu W, Zhang Y. The association of osteoprotegerin and RANKL with osteoporosis: A systematic review with Meta-Analysis. *J Orthop Surg Res*. 2023;18:839. <https://doi.org/10.1186/s13018-023-04179-5>.
- Zhang L, Liu M, Zhou X, Liu Y, Jing B, Wang X, Zhang Q, Sun Y. Role of osteoprotegerin (OPG) in bone marrow adipogenesis. *Cell Physiol Biochem*. 2016;40:681–92. <https://doi.org/10.1159/000452580>.
- Wan Y, Hu C, Hou Y, Si C, Zhao Q, Wang Z, Wang L, Guo X. OPG Gene-Modified Adipose-Derived stem cells improve bone formation around implants in osteoporotic rat maxillae. *Heliyon*. 2023;9. <https://doi.org/10.1016/j.heliyon.2023.e19474>.
- Ding M, Chen Z, Cho E, Park S-W, Lee T-H. Crucial role of Lysine-Specific histone demethylase 1 in RANKL-Mediated osteoclast differentiation. *Int J Mol Sci*. 2023;24:3605. <https://doi.org/10.3390/ijms24043605>.
- Siddiqui JA, Partridge NC. Physiological bone remodeling: systemic regulation and growth factor involvement. *Physiol (Bethesda)*. 2016;31:233–45. <https://doi.org/10.1152/physiol.00061.2014>.

23. Oryan A, Kamali A, Moshiri A, Baghaban Eslaminejad M. Role of mesenchymal stem cells in bone regenerative medicine: what is the evidence?? *Cells Tissues Organs*. 2017;204:59–83. <https://doi.org/10.1159/000469704>.
24. Rohban R, Pieber TR. Mesenchymal Stem and Progenitor Cells in Regeneration: Tissue Specificity and Regenerative Potential. *Stem Cells International* 2017, 2017, 5173732. <https://doi.org/10.1155/2017/5173732>
25. Bolamperti S, Villa I, Rubinacci A. Bone remodeling: an operational process ensuring survival and bone mechanical competence. *Bone Res*. 2022;10:1–19. <https://doi.org/10.1038/s41413-022-00219-8>.
26. Perut F, Roncuzzi L, Gómez-Barrena E, Baldini N. Association between bone turnover markers and fracture healing in long bone Non-Union: A systematic review. *J Clin Med*. 2024;13:2333. <https://doi.org/10.3390/jcm13082333>.
27. Safarova Y; Umbayev, Bauyrzhan; Hortelano, Gonzalo; and, Askarova S. Mesenchymal Stem Cells Modifications for Enhanced Bone Targeting and Bone Regeneration. *Regenerative Medicine* 2020, 15, 1579–1594. <https://doi.org/10.2217/rme-2019-0081>
28. Mollentze J, Durandt C, S Pepper M. An in vitro and in vivo comparison of osteogenic differentiation of human mesenchymal stromal/stem cells. *Stem Cells Int*. 2021;2021(9919361). <https://doi.org/10.1155/2021/9919361>.
29. Wang L, Ruan M, Bu Q, Zhao C. Signaling pathways driving MSC osteogenesis: mechanisms, regulation, and translational applications. *Int J Mol Sci*. 2025;26:1311. <https://doi.org/10.3390/ijms26031311>.
30. Yanik SC, Baker AH, Mann KK, Schlezinger JJ. Organotins are potent activators of PPAR $\gamma$  and adipocyte differentiation in bone marrow multipotent mesenchymal stromal cells. *Toxicol Sci*. 2011;122:476–88. <https://doi.org/10.1093/toxsci/kfr140>.
31. Prentice KJ, Saksi J, Hotamisligil GS. Adipokine FABP4 integrates energy stores and counterregulatory metabolic responses. *J Lipid Res*. 2019;60:734–40. <https://doi.org/10.1194/jlr.S091793>.
32. Na S, Jh G. Bone remodeling: multiple cellular interactions required for coupling of bone formation and resorption. *Semin Cell Dev Biol*. 2008;19. <https://doi.org/10.1016/j.semcdb.2008.07.016>.
33. Tang J, Wang X, Lin X, Wu C. Mesenchymal stem Cell-Derived extracellular vesicles: A regulator and carrier for targeting Bone-Related diseases. *Cell Death Discov*. 2024;10:1–14. <https://doi.org/10.1038/s41420-024-01973-w>.
34. Wang Y, Wen J, Lu T, Han W, Jiao K, Li H. Mesenchymal stem Cell-Derived extracellular vesicles in Bone-Related diseases: intercellular communication messengers and therapeutic engineering protagonists. *Int J Nanomed*. 2024;19:3233–57. <https://doi.org/10.2147/IJN.S441467>.
35. Zhao P, Xiao L, Peng J, Qian Y-Q, Huang C-C. Exosomes derived from bone marrow mesenchymal stem cells improve osteoporosis through promoting osteoblast proliferation via MAPK pathway. *Eur Rev Med Pharmacol Sci*. 2018;22:3962–70. [https://doi.org/10.26355/eurrev\\_201806\\_15280](https://doi.org/10.26355/eurrev_201806_15280).
36. Park K, Ju W-C, Yeo J-H, Kim JY, Seo HS, Uchida Y, Cho Y. Increased OPG/RANKL ratio in the conditioned medium of Soybean-Treated osteoblasts suppresses RANKL-Induced osteoclast differentiation. *Int J Mol Med*. 2014;33:178–84. <https://doi.org/10.3892/ijmm.2013.1557>.
37. Kim JH, Kim K, Kim I, Seong S, Koh J-T, Kim N. The ATF3–OPG Axis contributes to bone formation by regulating the differentiation of osteoclasts, osteoblasts, and adipocytes. *Int J Mol Sci*. 2022;23:3500. <https://doi.org/10.3390/ijms23073500>.
38. Ignatius A, Schoengraf P, Kreja L, Liedert A, Recknagel S, Kandert S, Brenner RE, Schneider M, Lambris JD, Huber-Lang M. Complement C3a and C5a modulate osteoclast formation and inflammatory response of osteoblasts in synergism with IL-1 $\beta$ . *J Cell Biochem*. 2011;112:2594–605. <https://doi.org/10.1002/jcb.23186>.
39. Guo Q, Kang H, Wang J, Dong Y, Peng R, Zhao H, Wu W, Guan H, Li F. Inhibition of ACLY leads to suppression of osteoclast differentiation and function via regulation of histone acetylation. *J Bone Min Res*. 2021;36:2065–80. <https://doi.org/10.1002/jbmr.4399>.
40. Oh SJ, Gu DR, Jin SH, Park KH, Lee SH. Cytosolic malate dehydrogenase regulates RANKL-Mediated osteoclastogenesis via AMPK/c-Fos/NFATc1 signaling. *Biochem Biophys Res Commun*. 2016;475:125–32. <https://doi.org/10.1016/j.bbrc.2016.05.055>.
41. Zhan K, Liu R, Tong H, Gao S, Yang G, Hossain A, Li T, He W. Fetuin B over-expression suppresses proliferation, migration, and invasion in prostate Cancer by inhibiting the PI3K/AKT signaling pathway. *Biomed Pharmacother*. 2020;131:110689. <https://doi.org/10.1016/j.biopha.2020.110689>.
42. Zhang W, Wang X, Tian S, Wang J, Zhou A. Fetuin-B interacts with insulin Receptor- $\beta$  and promotes insulin resistance in retina cells. *Invest Ophthalmol Vis Sci*. 2024;65:16. <https://doi.org/10.1167/iovs.65.12.16>.
43. Liu J, Jia S, Yang Y, Piao L, Wang Z, Jin Z, Bai L. Exercise induced Meteorin-like protects chondrocytes against inflammation and pyroptosis in osteoarthritis by inhibiting PI3K/Akt/NF- $\kappa$ B and NLRP3/Caspase-1/GSDMD signaling. *Biomed Pharmacother*. 2023;158:114118. <https://doi.org/10.1016/j.biopha.2022.114118>.
44. Jung TW, Lee SH, Kim H-C, Bang JS, Abd El-Aty AM, Hacimüftüoğlu A, Shin YK, Jeong JH. METRNL attenuates Lipid-Induced inflammation and insulin resistance via AMPK or PPAR $\delta$ -Dependent pathways in skeletal muscle of mice. *Exp Mol Med*. 2018;50:1–11. <https://doi.org/10.1038/s12276-018-0147-5>.
45. Zhang L, Li Y, Wu Z, Shen Q, Zeng C, Liu H, Zhang X, Yang J, Liu Q, Tang D, et al. Metrnl inhibits choroidal neovascularization by attenuating the choroidal inflammation via inactivating the UCHL-1/NF- $\kappa$ B signaling pathway. *Front Immunol*. 2024;15:1379586. <https://doi.org/10.3389/fimmu.2024.1379586>.

## Publisher's note

Springer Nature remains neutral with regard to jurisdictional claims in published maps and institutional affiliations.